

Endohedrally confined helium: Study of mirror collapsesD. M. Mitnik,^{1,4} J. Randazzo,^{2,4} and G. Gasaneo^{3,4}¹*Instituto de Astronomía y Física del Espacio, and Departamento de Física, Facultad de Ciencias Exactas y Naturales, Universidad de Buenos Aires, C.C. 67, Suc. 28, (C1428EGA) Buenos Aires, Argentina*²*División Colisiones Atómicas, Centro Atómico Bariloche, (8400) S. C. de Bariloche, Río Negro, Argentina*³*Departamento de Física, Universidad Nacional del Sur, 8000 Bahía Blanca, Buenos Aires, Argentina*⁴*Consejo Nacional de Investigaciones Científicas y Técnicas, Argentina*

(Received 12 September 2008; published 3 December 2008)

The properties of a helium atom confined inside an endohedral cavity, such as a fullerene, are studied. The fullerene cavity is modeled by a potential well and the strength of this potential is varied in order to understand the collapse of different atomic wave functions into the fullerene cage. Three theoretical calculation methods have been developed: a relaxation method, a Sturmian basis method, and a variational method. The first two methods are nonperturbative. The three methods allow inclusion of full correlations among the two electrons. Results showing mirror collapse effects are presented for an *S*-wave model, in which all the angular quantum numbers are set to zero.

DOI: [10.1103/PhysRevA.78.062501](https://doi.org/10.1103/PhysRevA.78.062501)

PACS number(s): 31.10.+z, 37.30.+i, 31.15.vj

I. INTRODUCTION

One of the most fascinating features of the fullerene molecules [1] is that they are capable of enclosing atoms in their hollow interior, forming endohedrally confined atoms [2–4]. Experimental efforts have made it possible to trap atoms inside a fullerene in different ways [5–7]. The particular mechanisms responsible for the insertion of the atom, vary from a “brute force” implantation, to a “window” mechanism, in which high temperatures and pressures can break one of the carbon-carbon bonds in the cage. Small molecules and atoms can pass through this temporary hole, forming a stable endohedrally confined compound [8,9]. This confinement could have some unique advantages in isolating the atom from its environment, having applications as superconductors, drug-delivery agents, medical imaging compounds, or molecular containers. The study of atoms confined inside a hollow cage of carbon fullerene can also lead to important applications in nanostructure science and technology. It can be useful in a wide range of applications, from the study of storage of fuel cells [10], to a possible way to provide the building blocks for the qubits of a quantum computer [11].

Endohedrally confined helium (for example, He@C₆₀) has been produced in laboratories, by resistive heating or in electric arcs [12], by ion implantation [13], and in ion beam collision experiments [14]. The fact that it is extremely stable over long periods of time, leads to the search of this compound in different sediment and meteorite samples. Endohedrally confined helium molecules have been detected in clay sediments associated with the 65 million-year-old Cretaceous-Tertiary boundary [15]. In particular, the isotopic ratio of the trapped atoms ³He/⁴He, was found to be higher than the maximum reported mantle values, and similar to those found in some interplanetary dust particles. The implication is that the He within these fullerenes is of extraterrestrial origin. The largest of the mass extinction events in the Earth history, at the Permian-Triassic boundary (251 million years ago), wiped out 90% of ocean dwellers and 70% of plants, animals, and even insects, on land [16]. In 2001

Becker *et al.* [17] investigated sediments from this boundary section, looking for the presence of endohedrally trapped helium in fullerenes. They claimed that the unusual isotopic ratio of these helium atoms provides geochemical evidence that it was an impact event—probably an asteroid or a comet—that caused the extinction. Endohedrally confined helium in fullerenes, has even been extracted from shock-produced breccias associated with the 1.85 billion year old Sudbury Impact Crater (in Canada) [18]. These compounds may constitute the ultimate “time capsule.”

Concerning atomic physics, many studies have explored the response of the enclosed atoms to electromagnetic radiation. Photoionization of endohedral fullerenes is a subject of increasing interest (see, for example, Refs. [19,20], and references therein), rising to a number of interesting effects, such as confinement resonances [21], correlation confinement resonances [22], and interferences of resonances [23]. Experiments on photoionization of endohedral Sc₃N@C₈₀⁺ and Ce@C₈₂⁺ compounds by synchrotron radiation, are underway [24]. Regarding the system discussed in the present work, Amusia *et al.* [25] studied the two-electron photoionization cross section of the He@C₆₀ system at very high photon energies, a regime where correlation details about the structure of the wave functions can be neglected.

The detailed study of photoionization processes in encapsulated atoms brings up the necessity to analyze the atomic structure of these systems. The spectra of two-electron atoms under different kind of confinements—the simplest case that allows the study of changes in correlation effects—have been studied by many authors [26–29]. The ground-state properties of a confined helium atom by an endohedrally model potential with different potential parameters, have been studied by Neek-Amal *et al.* [30] by using a diffusion Monte Carlo method. It is expected that the atomic properties will be dramatically changed both quantitatively and qualitatively, from those characteristic of the free atoms. Dolmatov *et al.* [31] studied the impact of the confinement on various atomic features, such as the wave functions, energy levels, the filling of electronic shells, polarizability, photoabsorption and photo-

ionization, etc. In particular, they studied the phenomenon of “mirror collapse,” where an electron bound by the Coulombic potential falls into the outer potential well, but, at the same time, an excited level, having a bound orbital extended over the outer shell, collapses into the inner Coulombic attraction corresponding to the first level. These processes have been thoroughly studied for the endohedrally confined hydrogen atom [32].

We found, at first glance, that these effects were different in helium than in hydrogen confined systems. We examined stationary eigenvalues having two electrons in the outer shell, but it seems that the electrons in these configurations do not interact in any way with the inner electrons. We analyzed the evolution of the energy spectra as a function of the depth of the confining potential, and it was found to exhibit unusual level crossings. That contradicts the no-level crossing theorem, which states that a pair of energy levels connected by perturbation do not cross as the strength of the perturbation is varied [33]. The new questionable level ordering connote another strange consequence: the change in the number of nodes of the radial wave functions. It is easily shown [34] that for any one-dimensional potential the number of nodes is an adiabatic invariant (i.e., as the potential is being distorted continuously the number of nodes of any eigenfunction remains unaltered). That can not be true if the energy levels cross each other, as was found in our preliminary analysis. Therefore, we decided, before presenting the detailed spectroscopy of the system, that the study of the dependence of the energy levels on the strength of the confining potential, and effects such as the allowance or prohibition of the crossings and the changes in the number of nodes of the wave functions deserves particular consideration.

To this end, we developed three different computational methods in order to calculate accurate wave functions of the endohedrally confined He atom. Two of the methods are fully quantal nonperturbative, and account for the complete electron-electron correlations. The other method is a variational procedure that allows a fast evaluation of the wave functions. Significant simplifications allowing us to uncover rich variety of effects which can occur in confined systems rather than to make detailed precise predictions for a particular spectrum. Thus, we introduce a model potential to represent the fullerene cage. In order to understand the variations of the spectra of the confined He atom as a function of the confining potential, we focus first upon the S states. In particular, due to the fact that our goal at this stage is to obtain a general qualitative understanding, we have simplified our calculations and instead of dealing with the real helium atom, we calculate the spectra of the spherically symmetric model helium [35,36], also known as Temkin-Poet or the S -wave model for He.

Our work is organized as follows. In Sec. II we give a complete description of our theoretical methods. In Sec. III, we study the evolution of the energy spectrum as a function of the depth of the confining cage. Some conclusions are given in Sec. IV.

II. THEORY

Following the work of Connerade *et al.* [32], we model the endohedral environment by an attractive short-range

spherical shell with potential $V_w(r)$, given by

$$V_w(r) = \begin{cases} -U_0 < 0, & r_c \leq r \leq r_c + \Delta, \\ 0, & \text{otherwise,} \end{cases} \quad (1)$$

where r_c is the inner radius of the shell and Δ is the thickness of the shell. We use the values deduced by Xu *et al.* [37], $r_c=5.75$ a.u. and $\Delta=1.89$ a.u., which are specific for a C_{60} fullerene molecule. The value of U_0 , on the other hand, is changed from 0 to 10 a.u., in order to explore the general physics of the system, relevant to other means of confining the atom (for example, altering the number of carbon atoms in the fullerene cage).

The Hamiltonian for a nonrelativistic spherically symmetric model helium, trapped inside a fullerene hollow cage may be written (in atomic units) as

$$\begin{aligned} H(\vec{r}_1, \vec{r}_2) &= H(r_1, r_2) \\ &= -\frac{1}{2} \frac{\partial^2}{\partial r_1^2} - \frac{1}{2} \frac{\partial^2}{\partial r_2^2} - \frac{Z}{r_1} - \frac{Z}{r_2} + V_w(r_1) + V_w(r_2) + \frac{1}{r_{>}}, \end{aligned} \quad (2)$$

where $r_{>}$ denotes the larger of the two radii r_1 and r_2 . This is the simplest model for two electrons interacting with each other and with a nucleus via long-range Coulomb forces. In this model, both electrons r_1 and r_2 are restricted to spherical states, and all angular correlations are eliminated. Therefore, the full six-dimensional problem is reduced to a two-radial dimensional problem and no further distinction between the total wave functions and the radial wave functions will be made unless explicitly stated. However, this model retains most of the other features (and computational difficulties) associated with the full He calculation. Moreover, the S -wave model is quite a good approximation to the real helium for the bound $1sns$ configurations.

A. The relaxation method

In the work presented by Mitnik [38–40], a complete non-perturbative solution of the helium atom-in-a-box problem was presented by developing two numerical techniques. The first consists of the direct solution by diagonalization of the Hamiltonian, and the second is based on a constrained relaxation of the wave functions. In this work, the same procedure has been followed, though modifying the calculations to include the fullerene potential given by Eq. (1). In this method, the energies and wave functions are calculated by relaxation of an initial wave function φ in a fictitious imaginary time $\tau=it$. That means a transformation of the time-dependent Schrödinger equation into a diffusion equation

$$\frac{\partial \varphi(r_1, r_2, \tau)}{\partial \tau} = -H\varphi(r_1, r_2, \tau). \quad (3)$$

The solution of this equation is given by

$$\varphi(r_1, r_2, \tau) = e^{-H\tau} \varphi(r_1, r_2, 0). \quad (4)$$

Expanding the solution in terms of the time-independent energy-eigenvector basis

$$\begin{aligned}\varphi(r_1, r_2, \tau) &= \sum_{q=1}^{\infty} a_q \psi_q(r_1, r_2) e^{-E_q \tau} \\ &= e^{-E_1 \tau} \left(a_1 \psi_1(r_1, r_2) + \sum_{q=2}^{\infty} a_q \psi_q(r_1, r_2) e^{-(E_q - E_1) \tau} \right),\end{aligned}\quad (5)$$

where ψ_1 is the lowest energy eigenvector having the same symmetry as φ , and E_1 is its energy. Since $(E_q - E_1) > 0$, the net result from this imaginary time propagation is the enhancement of those components of the solution with smaller eigenvalues of H relative to those with larger eigenvalues. At the limit $\tau \rightarrow \infty$, $\varphi \rightarrow \psi_1$. Thus, after many iterations (renormalizing continuously the wave function), only the lowest level eigenvalue (i.e., the ground state, or the first metastable level, according to the parity of the initial function φ) survives from the relaxation. Higher eigenvectors are calculated by imposing constraints at the iteration of the relaxation which requires the state to be orthogonal, thus preventing its collapse to lower levels.

The computer codes which implement this method are also adapted to run on parallel computers. In this case the wave functions are partitioned over the many processors in such a way that the communications between the processors are minimized and performed at every time step only for the partitioned domain borders. This parallelization scheme is a standard procedure for many of the time-dependent close coupling (TDCC) different works (for example, Refs. [41,42]).

B. The variational method

Our variational approach is based on the angular correlated configuration interaction method implemented for helium and He-like ions presented in previous work [43,44]. We first generate the variational one-electron ground state wave function which are the approximate solution for the short-range attractive potential representing the endohedral environment, given in Eq. (1),

$$\phi_w = e^{-a(U_0)(r-r_0)^2}, \quad (6)$$

where $r_0 = r_c + \frac{\Delta}{2}$ is the position of the center of the potential well. The parameter $a(U_0)$ is obtained by minimizing the energy of this level, invoking the variational principle. We calculate the value of these parameters as a function of different potential depths, obtaining a smooth and simple analytical function. The ‘‘well solution’’ function ϕ_w is combined with the atomic wave functions forming the following basis functions:

$$\chi_1(r_1, r_2, r_{12}) = \varphi_{1s}(r_1) \varphi_{1s}(r_2) \left(1 + \frac{r_{12}}{2} \right), \quad (7)$$

$$\chi_2(r_1, r_2, r_{12}) = [\varphi_{1s}(r_1) \phi_w(r_2) + \phi_w(r_1) \varphi_{1s}(r_2)] \left(1 + \frac{r_{12}}{2} \right), \quad (8)$$

$$\chi_3(r_1, r_2, r_{12}) = [\varphi_{1s}(r_1) \phi_w(r_2) - \phi_w(r_1) \varphi_{1s}(r_2)] \left(1 + \frac{r_{12}}{2} \right), \quad (9)$$

$$\chi_4(r_1, r_2, r_{12}) = \phi_w(r_1) \phi_w(r_2) \left(1 + \frac{r_{12}}{2} \right), \quad (10)$$

where $\varphi_{1s}(r)$ is the solution of the ground state of the hydrogenic ion with charge $Z=2$. The basis functions itself are combined

$$\psi^n(r_1, r_2, r_{12}) = \sum_k^4 c_k^n \chi_k(r_1, r_2, r_{12}) \quad (11)$$

and, in this way, we can obtain the four lowest-energy solution of the system. As is well known, the variational coefficients c_k^n from Eq. (11) are obtained, together with the energy levels E_n , by solving the generalized eigenvalue problem [45]

$$\sum_i [\hat{H} - E_n \hat{S}] c_k^n = 0, \quad (12)$$

where \hat{H} is the Hamiltonian matrix

$$H_{ij} = \langle \chi_i | \hat{H} | \chi_j \rangle, \quad (13)$$

and \hat{S} is the overlap matrix

$$S_{ij} = \langle \chi_i | \chi_j \rangle. \quad (14)$$

Here we have used a small number of basis functions (only four) to study the problem. However, we can a larger number of basis functions, increasing significantly the accuracy of the results [44]. It is important to remark that in the work performed by Neek-Amal *et al.* [30], similar wave functions have been proposed for the variational calculation. However, they did not take into account functions such as our χ_4 in which both electrons can be trapped inside the fullerene cage. Therefore, a full family of curves was overlooked in they discussion of the ground state spectra as a function of the confining potential strength.

C. The Sturmian method

The main aspects of the Sturmian method employed here has been published in a previous work [46]. We will give here just a short introduction to the theoretical procedure utilized in the present work. We have generated a one-electron Sturmian basis set S_n which are the solutions of the equation

$$\left[-\frac{1}{2} \frac{d^2}{dr^2} + V_0(r) - \epsilon \right] S_n(r) = -\beta_n V(r) S_n(r), \quad (15)$$

together with the physical boundary conditions

$$\begin{cases} S_n(r) \rightarrow 0 & r \rightarrow 0, \\ S_n(r) < \infty & r \rightarrow \infty. \end{cases} \quad (16)$$

In this case, the one-electron energy ϵ is considered as a fixed parameter and the effective charges β_n are the eigen-

values to be determined. This is in contradistinction with the normal approach to solve the Schrödinger equation where the charge is fixed, and the energy values are required. The potential $V_0(r)$ is an adequate model potential representing the central potential wherein the bounded electron moves, and $V(r)$ is any short range central potential. In our case we have chosen

$$V_0(r) = -\frac{Z}{2r} + V_w(r) \quad (17)$$

and

$$V(r) = -\frac{e^{-\lambda r}}{r}, \quad (18)$$

where $V_w(r)$ is the well potential given in Eq. (1), representing the fullerene cage, and λ is a free parameter. If the potential $V(r)$ vanishes at distances $r > a$, the whole set of wave solutions of Eq. (15) represent an electron of energy ϵ moving in the outer region of the potential V_0 . To solve the radial equations (15), two approaches were studied. In the first approach [46], the functions S_n are expanded in a complete L^2 -basis set formed by Laguerre-type functions. This allows us to write many of the integrals needed to solve the equations in a simple analytical form. In the second approach [47], we solve the radial equations by using a numerical five-point finite differences method.

The one-electron Sturmian basis set S_n are used, in turns, to construct a two-electron basis set for the study of two-electron atomic systems

$$\Phi_\alpha^S(r_1, r_2) = \mathcal{A}_S \frac{S_{n_1}(r_1)}{r_1} \frac{S_{n_2}(r_2)}{r_2}, \quad (19)$$

where the operator \mathcal{A}_S

$$\mathcal{A}_S F(r_1, r_2) = \frac{1}{\sqrt{2}} [F(r_1, r_2) + (-1)^S F(r_2, r_1)] \quad (20)$$

is introduced in order to satisfy the Pauli exclusion principle according to the spin state being considered.

The basis set elements Φ_α are combined in the form

$$\psi^S(r_1, r_2) = \sum_\alpha a_\alpha^{LS} \Phi_\alpha^S(r_1, r_2) \quad (21)$$

and the solution of the two-electron Schrödinger equation

$$H(r_1, r_2) \Phi_\alpha^S(r_1, r_2) = E \Phi_\alpha^S(r_1, r_2) \quad (22)$$

is translated into a generalized eigenvalue problem

$$[\mathbf{V}^{12} - \mathbf{V}^1 - \mathbf{V}^2] \mathbf{a} = \tilde{E} \mathbf{S} \cdot \mathbf{a}, \quad (23)$$

where the matrix elements of the different operators are

$$V_{\alpha,\beta}^{12} = \langle \Phi_\alpha^S | \frac{1}{r_{>}} | \Phi_\beta^S \rangle, \quad (24)$$

$$V_{\alpha,\beta}^i = \langle \Phi_\alpha^S | \beta_{n_i} V(r_i) | \Phi_\beta^S \rangle, \quad (25)$$

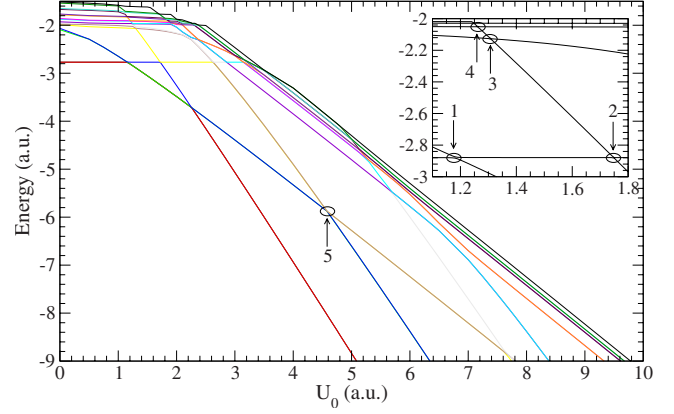


FIG. 1. (Color online) Energy levels for the endohedrally confined S -wave helium, for different confining potential depths. Inset: Energies for the first singlet levels. Label points for further detailed analysis.

$$S_{\alpha,\beta} = \langle \Phi_\alpha^S | \Phi_\beta^S \rangle, \quad (26)$$

and the total energy of the level $E = \tilde{E} + \epsilon_1 + \epsilon_2$. Note the absence of the kinetic and long-range potential parts in Eq. (23). This is a consequence of the use of the Sturmian basis, which cancels these terms analytically (see Refs. [46,47] for details).

III. RESULTS

A. Comparison between the different methods

The calculated spectra as a function of the confining potential depth is shown in Fig. 1. The curves correspond to the first ten levels obtained by using the relaxation method of calculation. Since the curves corresponding to triplet states are indistinguishable with the corresponding singlet curves, we only plotted, in the present figure, the singlet states. In the inset, a detailed portion of the spectra is shown, and in this case, the results have been obtained by using the Sturmian basis set calculation method.

In principle, the methods outlined in the previous section are very accurate, and we can obtain, in both nonperturbative methods, solutions with arbitrary precision. However, our intention in the present work has not been to obtain the best energies and wave functions. Instead, we are interested in presenting a complete solution to the problem which could be used to understand the nature and physical significance of many-body interactions in confined atomic systems.

Although we are not making a fair comparison among the three calculation methods, we will outline briefly the computational sizes and the results given by each of them. The variational method is very fast and simple and obtains the most important physical features of the wave functions. In this particular work, using only four functions for constructing the basis set described in Eq. (11), an energy value for the Temkin-Poet helium ground state of $E_{1s^2} = -2.804$ a.u. was obtained. A complete discussion of the convergence of the energy values with different basis set size is given in Refs. [43,44], where we show that very good energy values

can be obtained with a few tens of functions in the basis.

For the relaxation method, we have computed first the ground state of the S -wave model He with different numerical grids in order to check the sensitivity and convergence of the calculations. The energy of the $1s^2$ level, obtained with a numerical grid having a mesh spacing $\Delta r=0.2$ is $E_{1s^2}=-2.759$ a.u., compared with the best value available on the literature of -2.8790288 a.u. (with other 14 digits that are not relevant in our comparisons) obtained by Goldman [48]. It is important to notice that for this numerical lattice, the one-electron energy of the He^+ $1s$ level is $\epsilon_{1s}=-1.926$ a.u., compared to the exact value of -2.000 a.u. For the results shown in Fig. 1 we have performed a better calculation, with a mesh size of $\Delta r=0.15$ a.u., where $\epsilon_{1s}=-1.9569$ a.u., obtaining a ground-state energy of $E_{1s^2}=-2.809$ a.u. Better energies can be generated by decreasing the mesh step size and increasing the number of points. Convergence is demonstrated by using a grid with $\Delta r=0.075$ a.u., where $\epsilon_{1s}=-1.9889$ a.u. and $E_{1s^2}=-2.861$ a.u., and with $\Delta r=0.01$, in which $\epsilon_{1s}=-1.9998$ a.u. and $E_{1s^2}=-2.8787$ a.u.

For the Sturmian method, the different wavefunctions have been generated by using 65 one-electron Sturmian functions $S_n(r)$, which leads to 2145 basis functions $\Phi_a(r_1, r_2)$ per symmetry S . These basis functions extend until a range of 80 a.u. Using this function set, we obtained an energy value of $E_{1s^2}=-2.8790294$, in excellent agreement with Goldman's value. The convergence of the method is discussed in Ref. [47], and in this particular case, we can reach accuracies of $\approx 10^{-8}$ by using 105 one-electron Sturmian functions. Due to the high precision reached with relatively low computational cost, the Sturmian method will be the calculation method used in the rest of the paper.

B. Avoided crossings and mirror collapses

Roughly speaking, the horizontal lines shown in the previous figure represent unperturbed binding in the inner (atomic) well, while the diagonal lines represent binding in the outer well. The main feature noticeable in the spectra is that there are only two kinds of asymptotic behavior, and both are linear. The different slopes of this linear dependence correspond to one or two electrons confined in the spherical well of the confining potential (this is also confirmed by the fact that one slope is exactly twice as steep as the other). As the confining potential increases not only do the energy levels change, but the shape of the wave functions are also drastically modified. That means that any physical process involving the functions, either in the initial or final state of the process, will be altered even more dramatically than the energy level structure.

In the following, we will analyze the behavior of the lowest level. This level is $1s^2$ for small values of U_0 , and its energy remains $E_{1s^2}=-2.879$ a.u., the bounding energy of the free S -wave He. This is because the extent of the $1s^2$ radial wave function is such that it is essentially zero at the inner radius of the confining potential well. Therefore, for small U_0 it does not "feel" the effects of the outer confining well. The $1s2s$ state, on the other hand, has a significant portion of its amplitude in the region of the confining well and, thus,

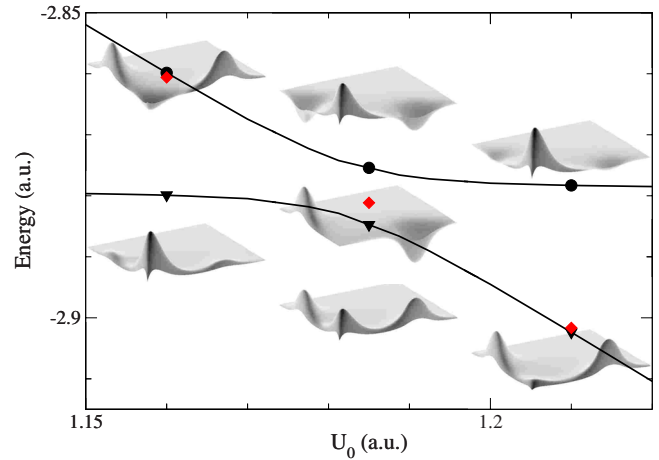


FIG. 2. (Color online) First three wave functions $1s^2 1S$, $1s\phi_1 1S$, and $1s\phi_1 3S$ for different potential depths, around the first avoided crossing at $U_0 \approx 1.185$ a.u.

one of the electrons very quickly gets bound in this outer well. The wave function then becomes $1s\phi_1$, where ϕ_1 denotes the wave functions representing one electron in the ground state of the square well potential. The energy of this state decreases as the outer well deepens. With further deepening of the outer well, the $1s\phi_1$ state has energy comparable with the $1s^2$ state. At this point of degeneracy, a strong interaction between the two states leads to avoided crossing, clearly seen at a potential well amplitude of $U_0=1.15$ a.u. The wave functions corresponding to the first three energy levels are displayed in Fig. 2, together with the curves corresponding to the $1s^2 1S$, $1s\phi_1 1S$, and $1s\phi_1 3S$ energy levels. As expected, the figure shows that in the $1s^2$ both electrons are trapped in the inner (Coulombic) potential, while in the levels $1s\phi_1$ one electron is trapped in the inner potential, whereas the other is trapped in the outer-fullerene cage. Among all the crossings studied in the present work, this is the only one in which the repulsion between the different configurations, and hence, the avoidance of the crossing, is clearly noticeable. The figure shows that at a value of the confining potential $U_0=1.15$ a.u., the lowest level $1s^2$ begins to suffer the influence of the outer potential. This is detectable as the two protuberances at the tail of the wave function, having a maximum at a radius that corresponds to the center of the fullerene potential well. On the other hand, at the same potential, the wave function corresponding to $1s\phi_1 1S$ (higher energy level), is also perturbed by the lowest energy level wave function, showing a deep noticeable feature around the origin. At $U_0=1.185$ the interaction between these two levels reaches the maximum closeness between them. The energy of the $1s\phi_1 1S$ is -2.884 a.u., whereas the energy of the $1s^2 1S$ is -2.876 a.u. At a slightly deeper potential $U_0=1.21$ a.u., the characteristic shapes of the wave functions are inverted. The higher energy level becomes a $1s^2$ function, since the amplitude at the origin is much higher than the amplitude at the outer potential cage. On the other hand, the probability at the origin for the lowest energy level decreases drastically, in favor of giving a high probability at the cage position. The variational calculation allow us to clearly see what we have described. The coefficients c_1^1 and c_2^1 in Eq.

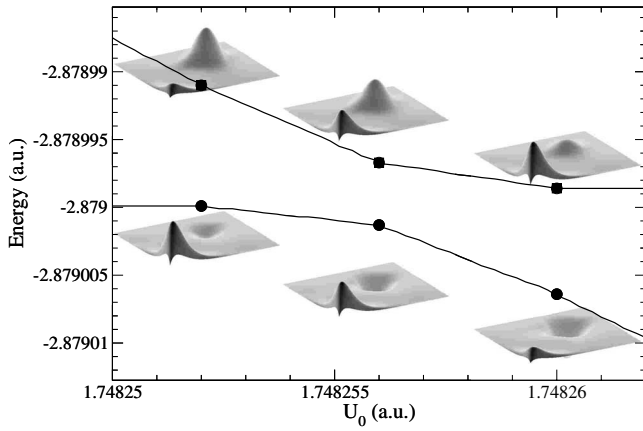


FIG. 3. $1s^2$ and $\phi_1^2 1S$ wave functions for different potential depths, around the avoided crossing labeled as 2 at $U_0 \approx 1.748$ a.u.

(11)—corresponding to the χ_1 (two electrons in the ϕ_{1s}) and χ_2 (a $\phi_{1s}\phi_1$ function) components of the lower level—are approximately 1 and 0, respectively, for very small values of U_0 . They exchange their values being close to 0 and 1, respectively, for $U_0 \approx 1.21$ a.u. (the coefficients for the other functions χ_3 and χ_4 are negligible). The same phenomena, but in the opposite way, is observed in the values of the coefficients c_1^2 and c_2^2 , for the first excited level. The diamond points in the figure represent the energy of the $1s\phi_1^3 S$ level at the different potential strengths. We only plotted the wave function for one of the points, since its shape does not change along the points. The reason for that is the different symmetry, that forbids the interaction with the singlets.

As a second example, we show in Fig. 3 the avoided crossing labeled as 2 in Fig. 1, in which the $1s^2$ level becomes degenerate with the $\phi_1^2 1S$ level. The former level is a state in which both electrons are trapped at the outer potential well. As seen in the figure, both energy levels reach the closest approach at $U_0 = 1.748255$ a.u., interchanging smoothly the probabilities of both electrons simultaneously. This means that below the potential of closest approximation ($U_0 < 1.748250$ a.u.), the higher energy level has both electrons in the outer potential well, whereas the lower has both

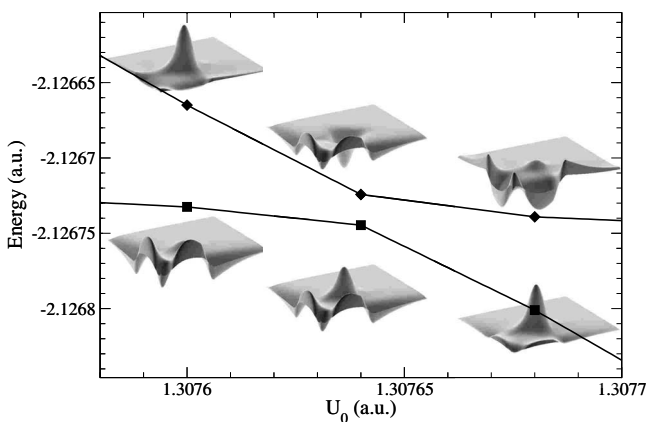


FIG. 4. $\phi_1^2 1S$ and $1s3s^1 S$ wave functions for different potential depths, around the avoided crossing at $U_0 \approx 1.30765$ a.u.

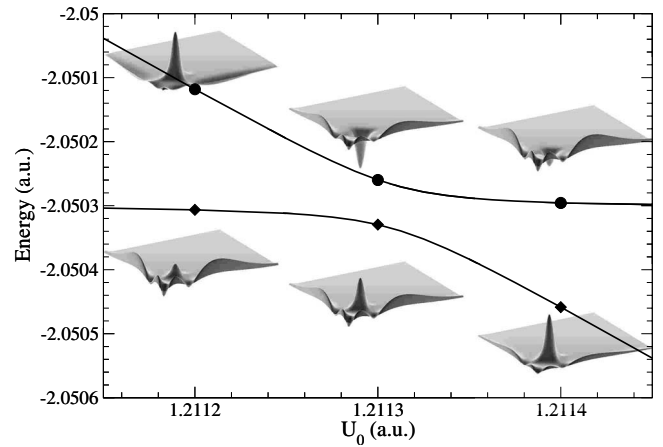


FIG. 5. $\phi_1^2 1S$ and $1s4s^1 S$ wave functions for different potential depths, around the avoided crossing at $U_0 \approx 1.26195$ a.u.

electrons around the nucleus. At $U_0 = 1.748255$ a.u. the wave functions become bimodal, as a result of being shared between two wells. Hybrid behavior results from dilating the inner atomic orbitals from their normal positions into a more external well. Notice that this incomplete orbital collapse is not a combination of one electron in the inner Coulombic well and the other in the outer fullerene cage, but the combination of two different states where in each one of them, both electrons share the same place. The probabilities interchange smoothly, and beyond the point shown in the figure ($U_0 > 1.748260$ a.u.), the higher energy level corresponds to the configuration with two electrons in the nucleus whereas the lower has the two electrons in the outer part. It is remarkable the high-energy precision needed in order to show the avoided characteristic of this crossing. In this case, only by calculating the energy levels with a resolution better than 10^{-5} a.u. can we conclude with certainty that the levels do not cross each other, but form an avoided crossing.

The wave functions for other levels at values of U_0 around the avoided crossings labeled as 3 and 4 in Fig. 1 are shown in the following Figs. 4–7. Figures 4 displays the avoided crossing number 3, which corresponds to the intersection of the $\phi_1^2 1S$ and $1s3s^1 S$ wave functions. The $1s3s$

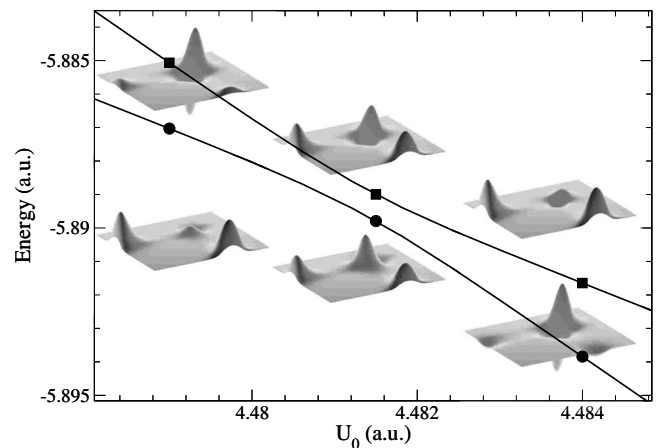


FIG. 6. $1s\phi_1^1 S$ and $\phi_1\phi_2^1 S$ wave functions for different potential depths, around the avoided crossing at $U_0 \approx 4.481$ a.u.

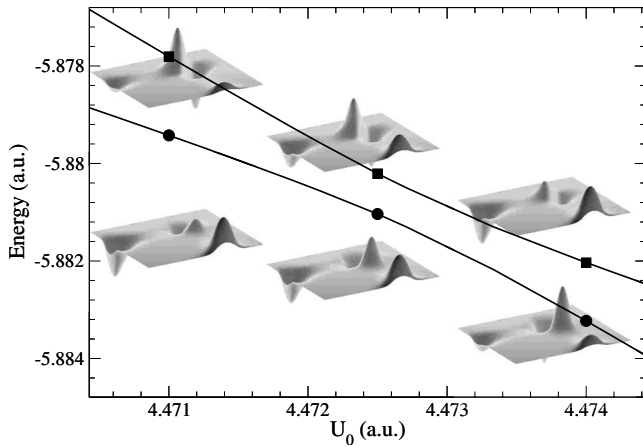


FIG. 7. $1s\phi_1^3S$ and $\phi_1\phi_2^3S$ wave functions for different potential depths, around the avoided crossing at $U_0 \approx 4.4725$ a.u.

wave function extends over the potential well, and the strength of the potential already allows an excited state bounded inside the well [for the particular well chosen in our model, having a spatial width of $\Delta = 1.89$ a.u., the successive bound states appear at a potential depths of $U_{0n} = (n-1)^2 / (8\pi^2\Delta^2)$, for $n=1, 2, 3, 4, \dots$, i.e., at $U_0 \approx 0, 0.35, 1.38, 3.11, 5.53$ a.u., respectively]. Therefore, this is not a pure Coulombic function, but a mixture of the $1s3s$ with a ϕ_2 . We arrived at this conclusion comparing this wave function with the pure $1s3s$ wave function (i.e., for $U_0=0$). We found that the pure Coulombic function has a smooth and moderate transition from the second to the third antinode. However, the wave function at $U_0 \approx 1.25$ produces an abrupt jump at the position of the external well, suggesting the presence of an excited bound function. Another reason for speculating that it is not a pure Coulombic state is the fact that the energy of this level continues to decrease as the potential depth increases, and that does not happens with higher excited levels (unless a new bound state is allowed inside the well). As shown in the figure, this function intersects smoothly with the ϕ_1^2 , interchanging the positions of two electrons, from the Coulomb attraction to the external well, and vice versa. The same ϕ_1^2 interacts with higher $1sns^1S$ states, as seen, for example, in Fig. 5, where the avoided crossing number 4 is illustrated, showing the intersection with the $1s4s^1S$ wave function. Again, the same feature appears here, where the two electrons inside the external well exchange positions with the electrons at the $1s4s$ function. In order to see this transition as an avoided crossing, it is necessary to calculate the energy levels with a resolution better than 10^{-4} a.u.

A more interesting avoided crossings are shown at Figs. 6 and 7. In the first case, the $1s\phi_1^1S$ wave function (which, at this potential well strength becomes the first excited level), interacts with the $\phi_1\phi_2^1S$ state, in which two electrons are in the outer potential well, one in the lower energy state, but the other in the first excited state of the well. In this physical process the probabilities of different wave functions are once more exchanged, as in the previous cases, but now the state created inside the fullerene cage is an excited state. Therefore, the protuberance appearing at the center of the region

plotted has both positive and negative antinodes. The $\phi_1\phi_2^3S$ wave function, on the other hand, does not interact with any of the functions plotted here (since it has a different symmetry), but it does with the $1s\phi_1^3S$ wave function, and therefore, they also change their shape along the curves. The energies of the $1s\phi_1^3S$ are very similar to the energies of the $1s\phi_1^1S$, since the repulsion of both electrons (confined in different spacial regions) is roughly the same. However, there are differences between the singlet and triplet levels, for the $\phi_1\phi_2$ wave functions. For this case, the energy of the triplet levels are smaller than the singlet energies, due to the larger mean values of the electronic distances for antisymmetric spatial wave functions. That is illustrated in Fig. 7, where crossing number 5 is shown for the triplet states. The energy of the avoided crossing is very similar to the one in the singlet case, but it occurs at a slightly lower well potential (and at higher energies of the involved levels).

After analyzing the shape of the wave functions and the characteristics of the avoided crossings, we investigated whether the reordering of the energy levels changed the number of nodes of the wave functions. If one follows the same kind of wave function along the energy vs potential cage strength curves (for example, looking at the $1s^2$ -like function), their energy order changes at every avoided crossing. That should produce a change in the node number, keeping the required orthogonality of the solutions. On the other hand, following the same energy curve (instead of the same kind of function), implies an adiabatic change of an external parameter, therefore, the number of nodes should be invariant. In order to produce a quantitative analysis of these changes, we need first to define a way to count the number of nodes. The radial wave functions are two-dimensional functions, so it is necessary to count nodal surfaces, rather than node numbers. This is illustrated in the contour plots of Fig. 8, where the $1s^2$ wave function is plotted for different potential depths. First the wave function is plotted before the first avoided crossing ($U_0=1.16$ a.u.). At this potential strength, $1s^2$ is the ground level, therefore this is a nodeless wave function (only one nodal surface). The middle plot shows the $1s^2$ wave function at a potential just above the first avoided crossing ($U_0=1.21$ a.u.), where, as is shown in Fig. 2, the $1s^2$ function becomes the first excited level, having energy values higher than the new ground level $1s\phi_1$. A nodal curve appears, dividing the wave into two nodal surfaces. The last plot shows the $1s^2$ wave function at a potential just above the second avoided crossing ($U_0=1.74826$ a.u.). At this potential, the ϕ_1^2 function is the first excited state (see Fig. 3), therefore, we expect some changes in the number of nodes of the $1s^2$ function, which becomes the second excited level. Indeed, as shown in Fig. 8, the $1s^2$ wave function now has three nodal surfaces, separated by the two nodal curves. Very tiny negative antinodes develop at each of the two new nodal surfaces. Thus, we have found a valid method for identify the level order, consisting of counting the different nodal surfaces. That will give a signature to identify the energy order of any stationary eigenfunction.

C. Information entropies

The avoided crossing phenomena is a mechanism for the state energy reordering, manifested by the energy level re-

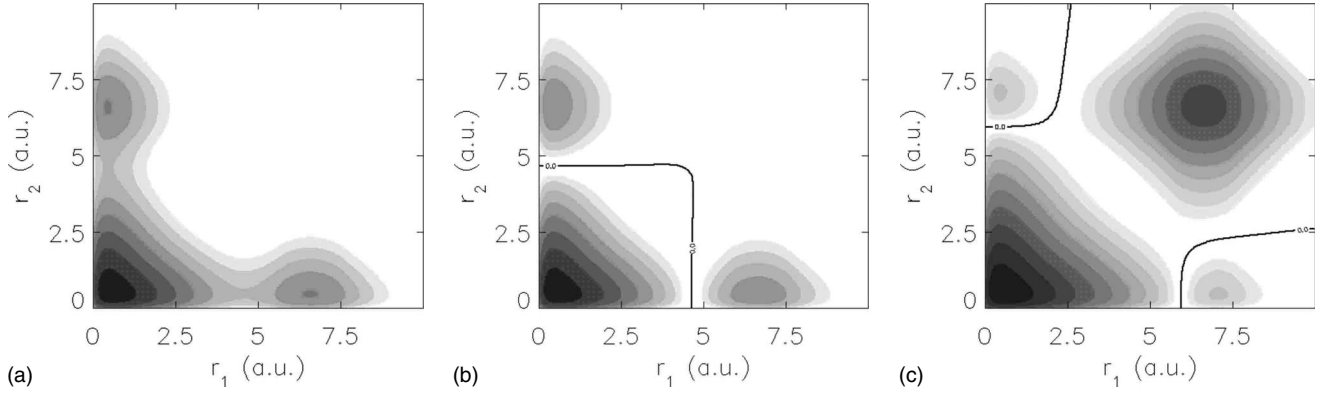


FIG. 8. Nodal surfaces for the $1s^2$ wave function, for different potential depths, around the successive avoided crossing at $U_0=1.16$, $U_0=1.21$, and $U_0=1.7482$ a.u.

pulsion: neighboring energy levels with the same symmetry do not cross each other, but rather come close and repel each other in an avoided crossing. An additional indicator of the external effects resides in the informational character. The states involved in the avoided crossings exchange their informational character. Therefore, it should be possible to estimate in a precise quantitative way the character exchange.

The Shannon information entropy of one-normalized electron density $\rho(\vec{r})$ in the coordinate space [49] is defined as

$$S_\rho = - \int \rho(\vec{r}) \ln \rho(\vec{r}) d\vec{r}. \quad (27)$$

This quantity is an information measure of the spatial delocalization of the electronic cloud. So, it gives the uncertainty of the localization of the electron. The lower this quantity, the more concentrated the wave function of the state, the smaller the uncertainty, and the higher the accuracy in predicting the localization of the electron. The variation of the Shannon entropy of states with an external potential strength may lead to gaining a deeper physical insight into the dynamics of the system through the avoided crossing region [50].

The existence of avoided crossings between states in the presence of the fullerene potential is manifest in the Shannon's entropy, as shown in Fig. 9(a). This figure displays the value of S_ρ along the different values of the external potential well, around the first avoided crossing, between the $1s^2$ and the $1s\phi_1$ wave functions. At the critical value of the confinement potential ($U_0=1.1073$ a.u.), a sudden change in both states occurs, provoking a drastic confinement of the electron cloud in one function, and the opposite in the other. An informational exchange between the states, which includes the exchange of the spatial localization or information-theoretic properties of the electron in going through this region, manifest in the abrupt changes in Shannon's entropies. The levels practically exchange their localization properties, as seen in the S_ρ values at any extreme of the curves.

A quantity related to the Shannon entropy, that also characterized the spreading of the wave function is the Shannon entropy power

$$J_\rho = \frac{1}{2\pi e} e^{(2/3)S_\rho}. \quad (28)$$

The changes in this quantity are shown in Fig. 9(b), having a behavior very similar to the Shannon entropy. However, the changes in J_ρ for these wave functions are of the order of 4, much higher than the changes in S_ρ . Therefore, it provides a more sensitive tool to characterize the information exchange.

The atomic avoided crossings can also be identified and characterized by means of another type of entropy information, the Fisher's information [51]. This provides another way to quantify the concentration of the probability density distribution of an electronic state $\rho(\vec{r})$

$$I_\rho = \int \frac{[\nabla \rho(\vec{r})]^2}{\rho(\vec{r})} d\vec{r} = 4 \int [\nabla \rho^{1/2}(\vec{r})]^2 d\vec{r}. \quad (29)$$

This information measures the spatial distribution of the quantum-mechanical probability cloud of a state in a manner qualitatively different but complementary to Shannon's en-

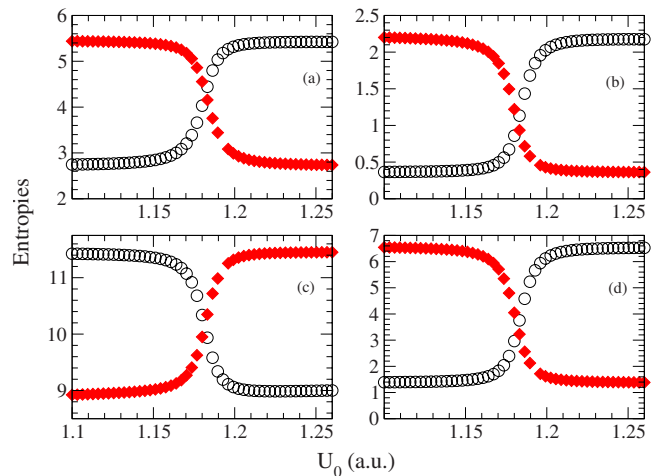


FIG. 9. (Color online) Information entropies for the lower levels around the first avoided crossing at $U_0=1.15$ a.u. (a) Shannon information entropies. (b) Shannon entropies power. (c) Fisher information entropies. (d) Fisher-Shannon information product entropies.

trophy. Both quantities characterize the information-theoretic content of the probability density describing a given physical state. Moreover, both can measure the disorder of the system at that state, i.e., the degree of smoothness of the probability density. However, the analytical properties of the two information quantities are quite different. The Shannon entropy is a logarithmic functional of the density, so that it is a global measure of disorder. The Fisher information is a gradient functional of the density, so it has a property of locality because it is sensitive to local rearrangements. Changes of I_ρ along the avoided crossing 1 are shown in Fig. 9(c). In this case, the higher (lower) energy level increases (decreases) the entropy as it passes across the avoided crossing. The Fisher information is also an information-theoretic measure of the spatial concentration of the electronic cloud. The higher this quantity, the more localized the state wave function, the smaller the uncertainty and the higher the accuracy in predicting the localization of the electron. Therefore, we can say that Shannon's entropy measures the spreading of the cloud and Fisher's entropy measures its concentration. The Shannon logarithmic functional best takes into account the tails of the probability distribution, while the Fisher gradient functional is more sensitive to local variations of the position of the electron.

An additional quantity, the Fisher-Shannon information product, defined as

$$P_\rho = \frac{1}{3} J_\rho I_\rho \quad (30)$$

was used as a tool for analyzing the electron correlation in an atomic system [52]. The changes in these entropy values along the first avoided crossing is shown in Fig. 9(d). At first sight it seems the same kind of behavior as the other entropies, but in this case the changes of P_ρ values are of the order of six. We found the information product the most sensitive tool to characterize the crossings, in all the cases studied in this work.

IV. CONCLUSIONS

The general behavior of an He atom confined in a variable fullerene cage has been analyzed. We have developed three different computational methods in order to solve the Schrödinger equation for an endohedrally confined He atom. Two of these methods are nonperturbative and provide very reliable solutions. The other is a very fast and simple variational approach, which gives the main physical features of the system. We used a potential model to account for the variation in the cage (for example, the number of carbon atoms in the fullerene), which allows one to understand the main physical effects of the external confinement in the atom. Avoided crossings are one of the most distinctive atomic spectroscopic features in the presence of an external parameter that is adiabatically changed. This is a consequence of the Von Neumann-Wigner noncrossing rule [53]. The influence of the external parameter variation (in our case the change in the potential strength of the external confinement cavity) is primarily reflected in the repulsion of the states. In this work we showed how the confinement potential strength affects in different amounts the atomic levels of the confined atom. Around the regions denoted as crossings, it seems that the variation in the potential produces degeneracies in energy, indicating that the levels can cross each to the other. A detailed analysis that requires a very high degree of precision shows that the energy levels do not cross each other, but rather come close and repel each other yielding to an avoided crossing. We analyzed the behavior of the avoided crossing levels by using different information entropies, providing an efficient tool to estimate in a physically transparent manner the atomic transitions caused by a slowly varying perturbation.

ACKNOWLEDGMENTS

This work has been supported partially by Grant No. PICTR03/00437 of ANPCYT, Grants No. PIP 5595 and No. PIP 6268 of CONICET, Grant No. PGI 24/F038 from Universidad Nacional del Sur, and Grant No. UBACyT X075 from Universidad de Buenos Aires, Argentina.

-
- [1] H. W. Kroto, J. R. Heath, S. C. O'Brien, R. F. Curl, and R. E. Smalley, *Nature (London)* **318**, 162 (1985).
 - [2] D. S. Bethune, R. D. Johnson, J. R. Salem, M. S. de Vries, and C. S. Yannoni, *Nature (London)* **366**, 123 (1993).
 - [3] H. Shinohara, *Rep. Prog. Phys.* **63**, 843 (2000).
 - [4] L. Forró and L. Mihály, *Rep. Prog. Phys.* **64**, 649 (2001).
 - [5] C. S. Yannoni, M. Hoinkins, M. S. de Vries, D. S. Bethune, J. R. Salem, M. S. Crowder, and R. D. Johnson, *Science* **256**, 1191 (1992).
 - [6] T. Kato, S. Suzuki, K. Kikuchi, and Y. Achiba, *J. Phys. Chem.* **97**, 13425 (1993).
 - [7] T. Almeida Murphy, T. Pawlik, A. Weidinger, M. Höhne, R. Alcalá, and J. M. Spaeth, *Phys. Rev. Lett.* **77**, 1075 (1996).
 - [8] M. Saunders, H. A. Jiménez-Vázquez, R. J. Cross, and R. J. Poreda, *Science* **259**, 1428 (1993).
 - [9] R. L. Murry and G. E. Scuseria, *Science* **263**, 791 (1994).
 - [10] L. Türker, *Int. J. Hydrogen Energy* **32**, 1933 (2007).
 - [11] W. Harneit, *Phys. Rev. A* **65**, 032322 (2002); S. C. Benjamin, A. Ardavan, G. A. D. Briggs, D. A. Britz, D. Gunlycke, J. Jefferson, M. A. G. Jones, D. F. Leigh, B. W. Lovett, A. N. Khlobystov, S. A. Lyon, J. J. L. Morton, K. Porfyrakis, M. R. Sambrook, and A. M. Tyrshkin, *J. Phys.: Condens. Matter* **18**, S867 (2006); Ju C. Chenyong, D. Suter, and J. Du, *Phys. Rev. A* **75**, 012318 (2007); W. Harneit, K. Huebener, B. Naydenov, S. Schaefer, and M. Scheloske, *Phys. Status Solidi B* **244**, 3879 (2007).
 - [12] T. Guo, R. E. Smalley, and G. E. Scuseria, *J. Chem. Phys.* **99**, 352 (1993).
 - [13] Z. Wan, J. F. Christian, Y. Basir, and S. L. Anderson, *J. Chem. Phys.* **99**, 5858 (1993).

- [14] K. A. Caldwell, D. E. Giblin, C. S. Hsu, D. Cox, and M. L. Gross, *J. Am. Chem. Soc.* **113**, 8519 (1991).
- [15] L. Becker, R. J. Poreda, and T. E. Bunch, *Proc. Natl. Acad. Sci. U.S.A.* **97**, 2979 (2000).
- [16] D. H. Erwin, *Sci. Am.* **275**, 72 (1996).
- [17] L. Becker, R. J. Poreda, A. G. Hung, T. E. Bunch, and M. Rampino, *Science* **291**, 1530 (2001).
- [18] L. Becker, J. L. Bada, R. E. Winans, T. E. Bunch, and B. E. French, *Science* **265**, 642 (1994).
- [19] A. S. Baltentkov, V. K. Dolmatov, and S. T. Manson, *Phys. Rev. A* **66**, 023201 (2002).
- [20] V. K. Dolmatov and S. T. Manson, *Phys. Rev. A* **73**, 013201 (2006).
- [21] V. K. Dolmatov, A. S. Baltentkov, J. P. Connerade, and S. T. Manson, *Radiat. Phys. Chem.* **70**, 417 (2004).
- [22] V. K. Dolmatov and S. T. Manson, *J. Phys. B* **41**, 165001 (2008).
- [23] M. Ya. Amusia, A. S. Baltentkov, and L. V. Chernysheva, *J. Phys. B* **41**, 165201 (2008).
- [24] A. Müller, S. Schippers, R. A. Phaneuf, M. Habibi, D. Esteves, J. C. Wang, A. L. D. Kilcoyne, A. Aguilar, S. Yang, and L. Dunsch, *J. Phys.: Conf. Ser.* **88**, 012038 (2007).
- [25] M. Ya. Amusia, E. Z. Liverts, and V. B. Mandelzweig, *Phys. Rev. A* **74**, 042712 (2006).
- [26] D. Bielińska-Waż, J. Karwowski, and G. H. F. Dierksen, *J. Phys. B* **34**, 1987 (2001).
- [27] R. Rivelino and J. D. M. Vianna, *J. Phys. B* **34**, L645 (2001).
- [28] B. Saha, T. K. Mukherjee, P. K. Mukherjee, and G. H. F. Dierksen, *Theor. Chem. Acc.* **108**, 305 (2002).
- [29] P. K. Mukherjee, J. Karkowski, and G. H. F. Dierksen, *Chem. Phys. Lett.* **363**, 323 (2002).
- [30] M. Neek-Amal, G. Tayebirad, and R. Asgari, *J. Phys. B* **40**, 1509 (2007).
- [31] V. K. Dolmatov, A. S. Baltentkov, J. P. Connerade, and S. T. Manson, *Radiat. Phys. Chem.* **70**, 417 (2004).
- [32] J. P. Connerade, V. K. Dolmatov, P. A. Lakshmi, and S. T. Manson, *J. Phys. B* **32**, L239 (1999).
- [33] J. J. Sakurai, *Modern Quantum Mechanics, Revised Edition* (Addison-Wesley, New York, 1994), p. 292.
- [34] E. Merzbacher, *Quantum Mechanics*, 2nd ed. (Wiley, New York, 1970), p. 68.
- [35] A. Temkin, *Phys. Rev.* **126**, 130 (1962).
- [36] R. Poet, *J. Phys. B* **11**, 3081 (1978).
- [37] Y. B. Xu, M. Q. Tan, and U. Becker, *Phys. Rev. Lett.* **76**, 3538 (1996).
- [38] D. M. Mitnik, D. C. Griffin, and M. S. Pindzola, *Phys. Rev. Lett.* **88**, 173004 (2002).
- [39] D. M. Mitnik, *Phys. Rev. A* **70**, 022703 (2004).
- [40] D. M. Mitnik, *Nucl. Phys. A* **790**, 784c (2007).
- [41] M. S. Pindzola, D. Mitnik, and F. Robicheaux, *Phys. Rev. A* **62**, 062718 (2000).
- [42] M. S. Pindzola, F. Robicheaux, S. D. Loch, J. C. Berengut, T. Topcu, J. Colgan, D. C. Griffin, C. P. Ballance, D. R. Schultz, T. Minami, N. R. Badnell, M. C. Witthoef, D. R. Plante, D. M. Mitnik, J. A. Ludlow, and U. Kleiman, *J. Phys. B* **40**, R39 (2007).
- [43] K. V. Rodriguez and G. Gasaneo, *J. Phys. B* **38**, L259 (2005).
- [44] K. V. Rodriguez, G. Gasaneo, and D. M. Mitnik, *J. Phys. B* **40**, 3923 (2007).
- [45] B. H. Bransden and C. J. Joachain, *Physics of Atoms and Molecules*, 2nd ed. (Prentice Hall, Englewood Cliffs, NJ, 2003), p. 130.
- [46] A. L. Frapiccini, V. Y. Gonzalez, J. M. Randazzo, F. D. Colavecchia, and G. Gasaneo, *Int. J. Quantum Chem.* **107**, 832 (2006).
- [47] J. M. Randazzo, A. L. Frapiccini, F. D. Colavecchia, and G. Gasaneo, *Int. J. Quantum Chem.* **109**, 125 (2009).
- [48] S. P. Goldman, *Phys. Rev. Lett.* **78**, 2325 (1997).
- [49] C. E. Shannon, *Bell Syst. Tech. J.* **27**, 623 (1948).
- [50] R. González-Férez and J. S. Dehesa, *Phys. Rev. Lett.* **91**, 113001 (2003).
- [51] R. A. Fisher, *Proc. Cambridge Philos. Soc.* **22**, 700 (1925).
- [52] E. Romera and J. S. Dehesa, *J. Chem. Phys.* **120**, 8906 (2004).
- [53] J. von Neumann and E. Wigner, *Phys. Z.* **30**, 467 (1929).